Mesoscale covariance of transport and CO2 fluxes: Evidence from observations and simulations using the WRF-VPRM coupled atmosphere-biosphere model

Ahmadov, R.; Gerbig, C.; Kretschmer, R.; Koerner, S.; Neininger, B.; Dolman, A.J.; Sarrat, C.

published in
Journal of Geophysical Research. Atmospheres
2007

DOI (link to publisher)
10.1029/2007JD008552

document version
Publisher's PDF, also known as Version of record

Mesoscale covariance of transport and CO_2 fluxes: Evidence from observations and simulations using the WRF-VPRM coupled atmosphere-biosphere model

R. Ahmadov,[1] C. Gerbig,[1] R. Kretschmer,[1] S. Koerner,[1] B. Neininger,[2] A. J. Dolman,[3] and C. Sarrat[4]

Received 16 February 2007; revised 18 July 2007; accepted 14 August 2007; published 30 November 2007.

[1] We developed a modeling system which combines a mesoscale meteorological model, the Weather Research and Forecasting (WRF) model, with a diagnostic biospheric model, the Vegetation Photosynthesis and Respiration (VPRM). The WRF-VPRM modeling system was designed to realistically simulate high-resolution atmospheric CO_2 concentration fields. In the system, WRF takes into account anthropogenic and biospheric CO_2 fluxes and realistic initial and boundary conditions for CO_2 from a global model. The system uses several ''tagged'' tracers for CO_2 fields from different sources. VPRM uses meteorological fields from WRF and high-resolution satellite indices to simulate biospheric CO_2 fluxes with realistic spatiotemporal patterns. Here we present results from the application of the model for interpretation of measurements made within the CarboEurope Regional Experiment Strategy (CERES). Simulated fields of meteorological variables and CO_2 were compared against ground-based and airborne observations. In particular, the characterization by aircraft measurements turned out to be crucial for the model evaluation. The comparison revealed that the model is able to capture the main observed features in the CO_2 distribution reasonably well. The simulations showed that daytime CO_2 measurements made at coastal stations can be strongly affected by land breeze and subsequent sea breeze transport of CO_2 respired from the vegetation during the previous night, which can lead to wrong estimates when such data are used in inverse studies. The results also show that WRF-VPRM is an effective modeling tool for addressing the near-field variability of CO_2 fluxes and concentrations for observing stations around the globe.

Citation: Ahmadov, R., C. Gerbig, R. Kretschmer, S. Koerner, B. Neininger, A. J. Dolman, and C. Sarrat (2007), Mesoscale covariance of transport and CO_2 fluxes: Evidence from observations and simulations using the WRF-VPRM coupled atmosphere-biosphere model, *J. Geophys. Res.*, *112*, D22107, doi:10.1029/2007JD008552.

1. Introduction

[2] Atmospheric measurements of CO_2 from global networks, mostly consisting of remote sites, have long been used in combination with inverse analysis to retrieve information on biosphere-atmosphere exchange rates and patterns [*Tans et al.*, 1990; *Gurney et al.*, 2002]. In order to retrieve information on regional scales, networks consisting of instrumented tall towers [*Bakwin et al.*, 1995] are currently being implemented over the continents. However, the location of the measurement sites close to variable sources is often located in meteorologically complex areas: terrain induced mesoscale phenomena such as sea-land, (lake, river, forest, etc.) breezes [*Pielke*, 2002], mountain-valley circulations, urban heat islands etc. make their representation in atmospheric models quite difficult. Such effects, which are usually on the subgrid scales of current generation transport models used in inversions, need to be studied with high-resolution mesoscale simulations that include CO_2 in order to bridge the gap between the measurements and inversion models. In fact, mesoscale models are essential in assessing the representation errors of coarse grid global models.

[3] Current modeling systems used for modeling of atmospheric CO_2 operate on three different scales. Global scale transport modeling is used in inverse mode to retrieve surface fluxes from observed mixing ratios [*Kaminski et al.*, 1999; *Peylin et al.*, 2005; *Rödenbeck et al.*, 2003], while regional [*Chevillard et al.*, 2002; *Gerbig et al.*, 2003] and mesoscale models [*Perez-Landa et al.*, 2006; *Lu et al.*, 2005; *van der Molen and Dolman*, 2007; *Sarrat et al.*, 2007a] are used currently for diagnostic purposes to better understand the mismatch between global scale models and measurements. With the development of high-performance computer clusters, and facilitated by parallelized codes,

[1] Max Planck Institute for Biogeochemistry, Jena, Germany.
[2] MetAir, Menzingen, Switzerland.
[3] Department of Hydrology and Geo-environmental Sciences, Vrije Universiteit Amsterdam, Amsterdam, Netherlands.
[4] CNRM Meteo France, Toulouse, France.

0148-0227/07/2007JD008552

high-resolution nonhydrostatic models are becoming increasingly used in contemporary meteorology and atmospheric chemistry.

[4] Mesoscale atmospheric processes have been shown to influence the atmospheric distribution of trace gases in different areas. Land-sea breeze circulation patterns for example play a role in the transport of atmospheric pollutants along coastlines, where elevated concentrations are recirculated in the sea-breeze [*Gangoiti et al.*, 2001]. *Perez-Landa et al.* [2006] studied the influence on CO_2 distribution of a combination of two mesoscale flows: sea breeze and up-valley circulations. According to their analysis, both a strong negative vertical gradient with increasing altitude, and a large horizontal gradient with higher values over the sea and lower values inland of the temporally averaged CO_2 concentration could be expected as a result of the combined mesoscale effects at the Western Mediterranean Basin scale.

[5] Recent work by *van der Molen and Dolman* [2007] concluded from mesoscale model simulations with RAMS [*Pielke*, 2002] that even relatively modest topography height differences can generate large horizontal gradients in CO_2 concentration to nighttime accumulation of CO_2 rich air at the foot of the mountains. They suggest that similar mesoscale gradients may be typical for almost all long-term observation stations of greenhouse gases.

[6] Therefore mesoscale atmospheric heterogeneity may have severe impact on the applicability of the methods to derive the regional-scale fluxes from CO_2 concentrations measurements. In order to investigate such situations for a large number of measurement locations with realistic representation of transport and biosphere-atmosphere exchange fluxes, we developed the WRF-VPRM modeling system. The WRF model [*Skamarock et al.*, 2005] is one of the widely used state-of-the-art models in mesoscale atmospheric modeling. In this paper we describe and apply a modeling system that couples WRF to the diagnostic biosphere model VPRM [*Mahadevan et al.*, 2007], which has shown remarkable skill in explaining both, temporal and spatial variability of CO_2 fluxes, without requiring any significant computational resources. VPRM is based on the MODIS satellite data (http://modis.gsfc.nasa.gov/) driven vegetation photosynthesis model VPM [*Xiao et al.*, 2004], but includes a component describing fluxes due to ecosystem respiration.

[7] To our knowledge, the work presented here is the first time that WRF is applied for CO_2 transport modeling. The benefit can be twofold: as accurate long-term measurements (better than 0.5 ppm) are available, modeling of CO_2 transport represents a critical test to verify WRF transport capabilities; on the other hand, given that transport is properly represented, the modeling system can be used to retrieve information about biospheric controls on the source-sink distribution from CO_2 measurements at much higher spatial and temporal resolution than achievable with current global models. On the global scale a Carbon Cycle Data Assimilation System (CCDAS) has been used to extract such process information [*Rayner et al.*, 2005], and we regard the work presented here as a significant step toward a regional scale assimilation system for CO_2.

[8] Thus the main goals of the work presented in this paper are (1) to develop a new mesoscale modeling tool in order to simulate CO_2 ort (by advection, turbulence and convection) at high vertical and horizontal resolution; (2) to simulate realistic biospheric CO_2 fluxes from different vegetation types with a diagnostic biosphere model that uses remotely sensed vegetation indices and modeled meteorological drivers; (3) to allow for separation of the different components of CO_2 in the model (biospheric uptake and respiration of CO_2, anthropogenic CO_2, advected global CO_2 fields); and (4) to analyze the ability of the coupled atmosphere-biosphere model to predict spatial and temporal variations of CO_2 by comparing it to airborne and ground-based measurements.

2. Modeling System Description

[9] The two major components of the modeling system are the WRF model and the VPRM model. Coupling between these components is realized by WRF providing near-surface temperature and shortwave downward radiation (SWDOWN) to VPRM, which returns fluxes of CO_2 to be used in WRF as a passive tracer. Further, as initial and lateral boundary conditions (ICs and LBCs) for CO_2 we used a global forward model results, and for anthropogenic CO_2 fluxes we used a high-resolution CO_2 emission inventory. The following sections 2.1–2.4 describe all of these components in detail.

2.1. WRF Model

[10] The major component of our modeling system is an atmospheric transport model. The WRF Model (http://wrf-model.org) is a next-generation mesocale numerical weather prediction system designed to serve both operational forecasting and atmospheric research needs. It is suitable for a broad spectrum of applications across scales ranging from meters to thousands of kilometers. The WRF model is designed to be a flexible, state-of-the-art, portable code that is efficient also in a massively parallel computing environment. WRF conserves mass, momentum, entropy and scalars by using flux form prognostic equations (W. C. Skamarock and J. Dudhia, The Advanced Research WRF (ARW) Dynamics Solver, WRF Tutorial Presentation, NCAR, 2006; avaibale at http://www.mmm.ucar.edu/wrf/users/tutorial/tutorial_presentation.htm). Taking into account all above mentioned we chose WRF (exactly Advanced Research dynamical core, WRF ARW 2.1.2 version) [*Skamarock et al.*, 2005] to simulate transport of CO_2 tracer in on-line mode. Here "on-line" means that CO_2 transport is performed concurrently with meteorological variables each time step (feedback of the rather small CO_2 variations of about 3% in column CO_2 on the radiation is neglected). One of the advantages of WRF is that it has a registry mechanism, which allows adding any kind of state variable (e.g., CO_2 concentration) that is declared during compilation in the subroutines involved (J. Michalakes, WRF software 2.1. WRF Tutorial Presentation, NCAR, 2006; available at http://www.mmm.ucar.edu/wrf/users/tutorial/tutorial_presentation.htm).

[11] For our study we used the WRF software and implemented tracers that are used to simulate CO transport in the MIRAGE experiment (http://box.mmm.ucar.edu/projects/mirage/, W. C. Skamarock, personal communication, 2006). We have done some modifications in order to include anthropogenic and biospheric CO_2 fluxes as well as

Table 1. Parameters and Physics Options Used in WRF Model

Category	Selected Options
Vertical coordinates	terrain-following hydrostatic pressure vertical coordinate
Basic equations	nonhydrostatic, compressible
Grid type	Arakawa-C grid
Time integration	3rd order Runge-Kutta split-explicit
Spatial integration	3rd and 5th order differencing for vertical and horizontal advection, respectively; both for momentum and scalars
Domain configuration	2 domains with resolution – 6 and 2 km for outer and inner domains, respectively; size 624 × 600 km and 330 × 234 km; 31 vertical levels for both domains up to 50 mb
Time step	36 and 12 s for outer and inner domains, respectively
Physics schemes	radiation: Rapid Radiative Transfer Model (RRTM) Longwave and Dudhia; microphysics: WSM 3-class simple ice scheme; cumulus: Kain-Fritsch (new Eta) scheme (only for the coarse domain!); PBL: YSU; surface layer: Monin-Obukhov; land-surface: NOAH LSM

initial and lateral boundary conditions (ICs and LBCs) for CO_2 concentration variables. Another specific detail is that we did not use the artificial filtering for the tracer variables. It is well known that high-order numerical schemes generate numerical noise and therefore tracers can get (unrealistic) negative values. But damping such signals lead to mass conservation violation that is not desirable. In the following we refer to the modified model code simply as WRF.

[12] All necessary meteorological data for initial and lateral boundary conditions, sea surface temperature (SST) and soil initialization fields of each run were taken from the ECMWF (http://www.ecmwf.int/) analysis data with about 35 km horizontal resolution and 6 hourly intervals. We avoided any local adjustment of parameterizations or specific local data to allow the model to be flexibly applied to other locations and times.

[13] To aid in tracking and distinguishing CO_2 signals from different sources, we implemented five types of "tagged" tracers for CO_2, which we will denote as C_{1-5}. These are C_1, total CO_2 concentration (which can be measured) that includes global CO_2 field and CO_2 tracers from anthropogenic and biospheric sources; C_2, only global CO_2, i.e., without any uptake or emission, which participates only in transport; C_3, anthropogenic CO_2; and C_4 and C_5, respiration and photosynthesis signals, respectively. All anthropogenic and biospheric fluxes were added at each simulation time step in CO_2 field to the lowest vertical level of the WRF grid. The tracer C_2 allows us to separate global CO_2 signal from the regional one. The main features of our WRF model system setup are presented in Table 1. Since the inner domain has 2 km resolution (meso-gamma scale), no cumulus parameterization was used, because such subgrid parameterizations are valid only for scales larger than about 5 km. On the other hand, convection is not really resolved explicitly, thus the chosen resolution is in a grey zone with respect to cumulus convection. In this sense we rely on periods with no cumulus activity, which was given for the periods considered here.

2.2. Initial and Lateral Boundary Conditions for CO_2 Fields

[14] As ICs and LBCs for total CO_2 and background CO_2 (C_{1-2}) fields we used LMDZ model data [*Peylin et al.*, 2005]. The global model has a horizontal resolution 1.25° (longitude), 0.83° (latitude) and 28 vertical levels up to the tropopause. Temporal resolution of the data is 1 hour. For anthropogenic and biospheric CO_2 (C_{3-5}) tracers ICs were zero. The standard WRF uses specified LBCs for a number of meteorological fields [*Skamarock et al.*, 2005]. We modified the WRF code to use such conditions for CO_2 fields as well. Thus specified LBCs were used for the outer domain to adjust to global fields from LMDZ (only for C_{1-2}) and for the inner domain with respect to outer coarse domain (for all C_{1-5}). A relaxation zone ensures that the LBCs are applied gradually over 5 grid cells.

[15] In the outer domain zero inflow and zero-gradient outflow LBCs were used for C_{3-5}. Depending on the wind direction this allows either tracers leave the domain easily, or it avoids artificial influx from "outside" for C_{3-5}. Since there is significant variability of CO_2 within the model domain that is at least partly resolved by the global model, using the global model fields as boundary conditions to the mesoscale tracer transport model is more accurate than using idealized profiles, which is typical for most of the traditional regional atmospheric chemistry models.

2.3. Anthropogenic CO_2 Fluxes

[16] Due to the spatial characteristic of fossil fuel emissions with strong emissions in populated areas and from power plants, a high spatial and temporal resolution inventory is required. Although for the considered spatial and temporal domain biospheric fluxes play a more important role in the domain of interest, anthropogenic fluxes are nevertheless necessary for interpretation of some experimental results (e.g., emission plumes encountered). We used a recently developed greenhouse gas emission inventory (updated in October 2005) from the Institute of Economics and the Rational Use of Energy (IER), University of Stuttgart (http://carboeurope.ier.uni-stuttgart.de/). The inventory contains hourly emission of greenhouse gases for 2000 year in 10 km resolution grid for European countries. We adopted these data for the year 2005 by taking into account the shift in week days between 2000 and the year of the simulation, preserving the temporal emission patterns (weekends versus week days). We rediscretized the fluxes on the WRF grids by conserving the total mass.

2.4. Biospheric CO_2 Fluxes

[17] One of the major parts of our model development work is the addition of VPRM to simulate biospheric CO_2 fluxes: photosynthesis and respiration fluxes. Generally there are different approaches to model CO_2 fluxes from vegetated areas, starting from highly simplified diagnostic models that use light and temperature sensitivity derived

from the eddy covariance observations [*Gerbig et al.*, 2003], and ending at sophisticated process-based ecophysiological models such as SiB2 [*Denning et al.*, 2003]. VPRM is a slightly more sophisticated diagnostic model that uses satellite indices, the land surface water index (LSWI) and the enhanced vegetation index (EVI) from MODIS satellite data at 500 meters resolution, shortwave radiative flux and air temperature data, to estimate the hourly Net Ecosystem Exchange (NEE) fluxes from different vegetation types [*Xiao et al.*, 2004; *Mahadevan et al.*, 2007]. The VPRM model was originally set up for the North American continent, with its four parameters optimized to fit eddy covariance measurements from AmeriFlux sites for different vegetation classes. We used VPRM with some modification for the areas in southern western Europe that comprises our modeling domain. As land-use data we used the SYNMAP [*Jung et al.*, 2006] data at 1 km resolution by reclassifying it into fractional vegetation using 8 groups. We used the VPRM parameter values from [*Mahadevan et al.*, 2007] with slight modifications to adapt it to the European sites. In future the eddy flux data will be used to derive more optimal parameter values for the European region.

[18] VPRM calculates NEE as a sum of Gross Ecosystem Exchange (GEE) and ecosystem Respiration (R). In our implementation, VPRM uses the same domains as WRF and calculates GEE using (1) SWDOWN and temperature at 2 meters (T2) provided by the WRF simulation in hourly interval; (2) EVI, which represents the fraction of shortwave radiation absorbed by leaves; and (3) the LSWI, which reflects changes in both leaf water content and soil moisture and accounts for the effects of leaf age on photosynthesis at the canopy level [*Xiao et al.*, 2004]. In addition VPRM takes into account the saturation of photosynthesis with increasing radiative flux. Respiration fluxes are calculated as a linear function of T2 from WRF [*Mahadevan et al.*, 2007]. VPRM calculated GEE and R fluxes are provided to WRF and transported as C_4 and C_5 tracers (also added on C_1) for respiration and photosynthesis.

[19] Although the VPRM is a relatively simple diagnostic model, it captures the spatiotemporal variability of biosphere-atmosphere fluxes remarkably well for temporal scales ranging from hours to years and for spatial scales from local scales (500 m, corresponding to eddy flux footprints) upward to continental scales [*Mahadevan et al.*, 2007]. The simple structure of the model allows readily validating it against observations at a large number of flux measurement sites within long time periods. Further, the limited number of parameters allows optimizing VPRM against CO_2 mixing ratio measurements in atmospheric inversion by using adjoint transport model such as STILT [*Gerbig et al.*, 2006; *Matross et al.*, 2006]. This provides a test of the upscaling methods from flux towers to regional scales.

[20] Oceanic CO_2 fluxes are neglected here because in the regional scale their contribution is insignificant compared to land [*Gerbig et al.*, 2003].

3. CERES Campaign

[21] Within the CERES project, which was a part of the CarboEurope Integra roject (http://carboregional.mediasfrance.org), an intensive observation campaign was performed in Les Landes, southwest France, May–June 2005 [*Dolman et al.*, 2006]. Les Landes region was chosen mainly because the heterogeneity is at large scale so that specific planetary boundary layer (PBL) structures may be identified with identifiable pieces of land cover. The main objective of the CERES was to determine spatial and temporal variability of CO_2 fluxes and concentrations at a regional scale. For this purpose a large number of different measurement methods and instruments were used during the campaign. Meteorological variables such as temperature, wind, humidity, turbulence fluxes, PBL height were measured during the campaign by automated stations, radiosoundings, ceilometers and aircraft. Surface energy fluxes, radiative fluxes as well as soil moisture and temperature were measured at a number of meteorological stations and eddy flux towers. CO_2 fluxes and concentrations were measured by eddy-flux towers, aircraft and a Fourier Transform Infrared (FTIR) instrument. The vast amount of data that was obtained during the campaign provides an invaluable opportunity for a model validation and data interpretation.

[22] One of the achievements of the campaign was the deployment of aircraft for both meteorological and atmospheric trace gas measurements, providing high-quality data with long temporal and spatial extension within and out of PBL. In this paper we used the data collected by MetAir's DIMO research aircraft (http://www.metair.ch), which performed overall 11 flights (42 hours) during the campaign. The aircraft was equipped with instruments to measure trace gases including CO_2, CO, NO, NO_2, NOy, O_3, and aerosols, as well as standard meteorological and navigational parameters [*Dolman et al.*, 2006]. CO_2 in-situ data from a modified closed path Licor 6262 [*Schmitgen et al.*, 2004] and an open-path Licor 7500 have been combined and adjusted to match the measurements of simultaneously collected flask samples; this is necessary since the continuous instrument is only calibrated on ground before and after, but not during each flight, and thus is not used as independent measurement. The combined record of high frequency but less precise open path, slower but more precise close path and accurate flask measurements give a 10 Hz response time series at an accuracy of 0.5 ppm. The suite of additional tracers has a strong potential to identify and to help quantifying pollution sources.

[23] CERES results showed clearly that at regional scale the relation between profiles and fluxes is strongly influenced by mesoscale flow patterns [*Dolman et al.*, 2006]. As a consequence, one has to consider synoptic and regional flows, fluxes and land surface in order to get a correct interpretation of the measured CO_2 concentration fields. The CERES data set with its high spatial and temporal coverage is used here as an initial application of the WRF-VPRM coupled atmosphere-biosphere modeling system.

4. Main Results and Discussion

[24] WRF was run for two domains with 2-way nesting option, with the coarse and inner domains shown in Figure 1. The domains contain different kind of land-use categories: ocean, forest, winter and summer crops, urban, and also mountains in the southern and eastern parts of the region.

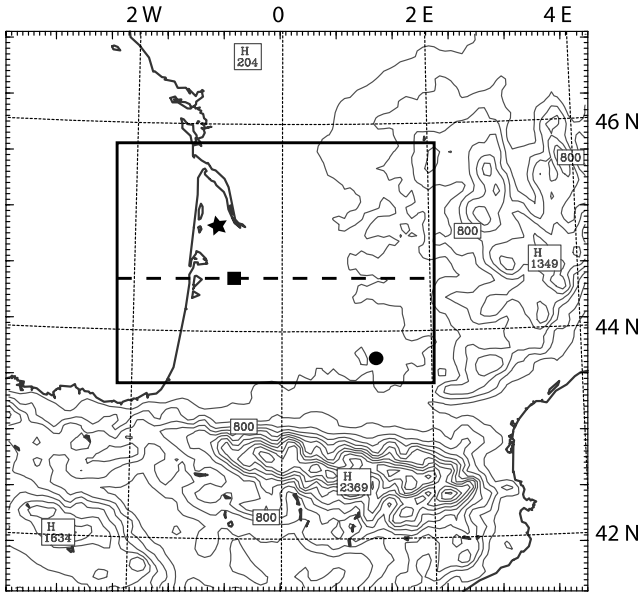

Figure 1. Terrain in the outer WRF-VPRM model domain. The smaller rectangle depicts the inner domain, and the dashed line is a WE cross section across La Cape Sud station. Three measurement stations, Bordeaux, La Cape Sud, and Toulouse, are shown with black star, square, and circle symbols, respectively.

Therefore the region is very interesting from the modeling point of view.

[25] We simulated CO_2 concentration distribution in the atmosphere by running WRF-VPRM for different days of the CERES campaign. Each run was done for 30 hours, starting at 18 UTC on the previous day, where first 6 hours of the simulation were used for spin-up. Note that all times are given in UTC; local time was UTC +2 hours. Here we present results for two days: 27 May and 6 June 2005. These days were also selected by different European modeling groups involved in CERES in order to set up an intercomparison exercise between different implementations of mesoscale models such as RAMS, MESO-NH and WRF [*Sarrat et al.*, 2007b]. 27 May was a very warm and slightly windy day, so the convective boundary layer development as well as CO_2 photosynthesis was very prominent in that day. The other day, 6 June, was slightly cloudier (cirrus) and moderately windy with west and northwest directions, but also with the development of a high PBL of around 1.5 km in the afternoon. During both days the aircraft measured meteorological parameters and CO_2 mostly profiling up and down in sawtooth mode along different flight trajectories, which provides a good opportunity to verify the modeling system for spatial scales of tens to hundreds of kilometers and over temporal scales spanning several hours. This section describes some analysis of the model results and their comparison to the measurements. It should be stated that all further demonstrated results are from the inner high-resolution domain (Figure 1). Nevertheless one should note that the outer coarse domain has also CO_2 transport and fluxes as the inner one, except it uses LBCs from the global models (for meteorology and CO_2) and we used this domain also for analyzing the ed results. The next sections discuss the modeling results in order to answer the following questions:

[26] 1. What does the model show as mesoscale circulation, and what is its impact on the CO_2 distribution?

[27] 2. Does it capture main features of the observed regional distribution of CO_2 concentration?

[28] 3. What can we learn from the model by distribution of CO_2 in different type of ''tagged'' tracers?

4.1. Case 1 (27 May 2005)

[29] During this day the area of southwest France was under the influence of an anticyclone, causing a weak wind mainly from southeast and clear skies. During the day the air was dry and very hot (the air temperature in Les Landes 34°C), and average surface winds were about 5–10 m/s.

[30] Results for the spatial distribution of CO_2 are presented together with vertical and zonal winds in Figure 2 as a zonal cross section (altitude versus longitude) along the latitude of the La Cape Sud (44°25′N, 00°34′W) measurement station (see the dashed line in Figure 1). In the cross section a distance of ≈50 km from the western corner belongs to the ocean, about 80 km inland is covered by pine forest and eastern part is a cropland area. The strong differences between the four different times indicate the large diurnal cycle of CO_2. During the night (0000 on 27 May, Figure 2a) CO_2 accumulates in a shallow nocturnal boundary layer, with SE wind transporting it toward the ocean. Nocturnal mixing ratios increase toward the morning and reach levels of more than 400 ppm, with a strong accumulation near the coastline due to the wind convergence (Figure 2b). The respired CO_2 is partially recirculated back toward the land during the morning due to a combination of upper westerly winds and the onset of a sea breeze (Figure 2c). However, since the CO_2 accumulation occurs mainly within the PBL, the sea breeze circulation has to be regarded as the main mechanism causing the recirculation in this case.

[31] In the afternoon, the CO_2 concentration is around 378 ppm over the ocean (Figure 2d), while only 50 km inland the concentration is higher by several ppm. At about 100 km farther inland the concentration drops by more than 10 ppm compared to the shore area, and a minimum mixing ratio is found around 180–200 km inland, with a CO_2 depletion of ≈15 ppm relative to the free atmosphere. The boundary layer height also shows gradients, reaching 1.5 km near the coast over forest, and less than 1 km farther inland over the cropland areas. The gradient in PBL height might be caused by the difference in the sensible heat flux, which is higher over the forest compared to the cropland area. However, this could also be caused by the sea breeze circulation, where an uplifting occurs near the coast. Farther inland, there are weaker horizontal CO_2 gradients over the cropland area also (Figure 2c) which is mainly due to differences in photosynthesis from the different crop types as will be discussed in section 4.3.

[32] To demonstrate these patterns in total CO_2, Figure 3a shows the horizontal distribution of near-surface CO_2 and wind vectors (hear near-surface means the center of the lowest vertical model level, which is ≈50–200 m above the ground) at 1400. Over the shore area the wind convergence can be seen as well as a large area of enhanced CO_2. This area extends to a few tens of kilometers inland, where

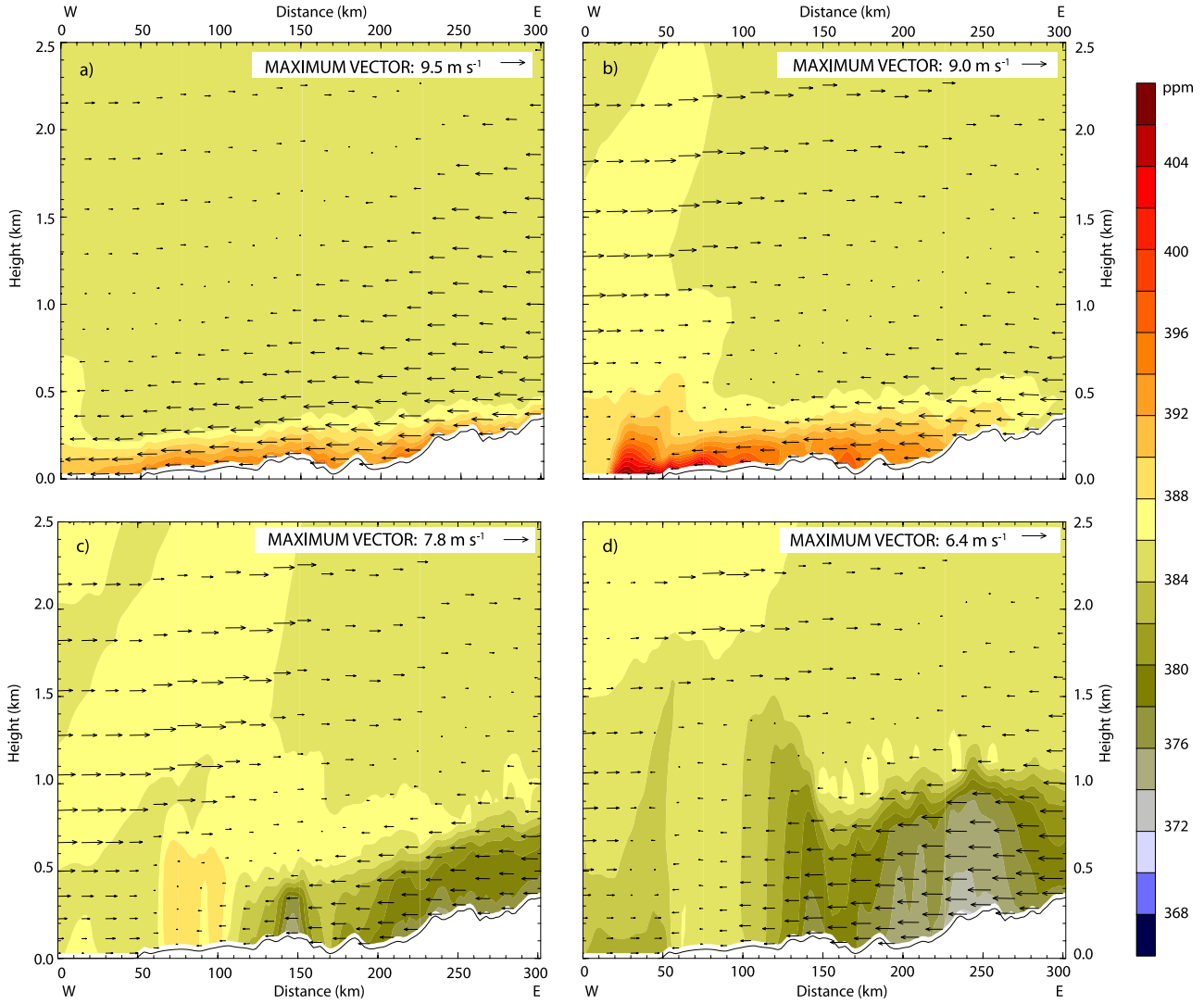

Figure 2. CO_2 distribution and wind vectors on the vertical plane along the dashed line in Figure 1, for the 27 May case, at (a) 0000, (b) 0600, (c) 1000, and (d) 1400.

strong decrease of CO_2 starts and covers almost all of the eastern part of the region. Over the ocean, near the coastline a turning of the low-level winds from southerly to southwesterly toward the coastline is found, which is clear evidence of the afternoon sea breeze. An interesting feature in the CO_2 distribution is the patch of relatively low concentration over the coastal ocean, which can also be recognized in the western part of Figure 2d. One may note that this plume did not yet arrive at this latitude at 1000 (see Figure 2c). This low CO_2 patch originates from photosynthesis over the vegetated land mainly in the bigger domain, and subsequent transport in NW direction followed by a change in wind direction toward Les Landes region in the afternoon. It is worth to note that a similar structure does not exist in the respired CO_2 field (Figure 3b).

[33] In order to further investigate the strong gradients near the coast, Figure 3b shows the spatial distribution of the tracer C4, i.e., the respired CO_2 signal also at the same time (1400). There are large plumes of respired CO_2 with a width of about 40 km, stretched along the coastline. Certainly the spatial st es evident in Figure 3b have to be caused by local respiration fluxes within the model domains, since we use zero influx for C4 (respired CO_2) at the lateral boundaries of the coarse grid. This clearly shows that air parcels with high CO_2 content "exported" from the land in the night returned back during the day by the onshore low-level winds. Since the mixing is weak over the ocean, and there are no surface fluxes (as mentioned before, they are neglected in the model), the CO_2 distribution over the ocean was essentially conserved. When these air parcels reached the land they mixed with the parcels moved from the inland with low CO_2 content due to the wind convergence in that area, thereby creating a strong spatial gradient.

[34] Our simple analysis revealed that the contribution from the anthropogenic emissions to the atmospheric CO_2 fields is marginal compared to the biospheric one, since the region is covered by active biosphere during this season. The main sources of the anthropogenic CO_2 in the region are two major cities, Bordeaux (44°50′N, 00°34′W) and Toulouse (43°36′N, 1°26′E), located in our domain; also there are other significant sources in the SW part of our

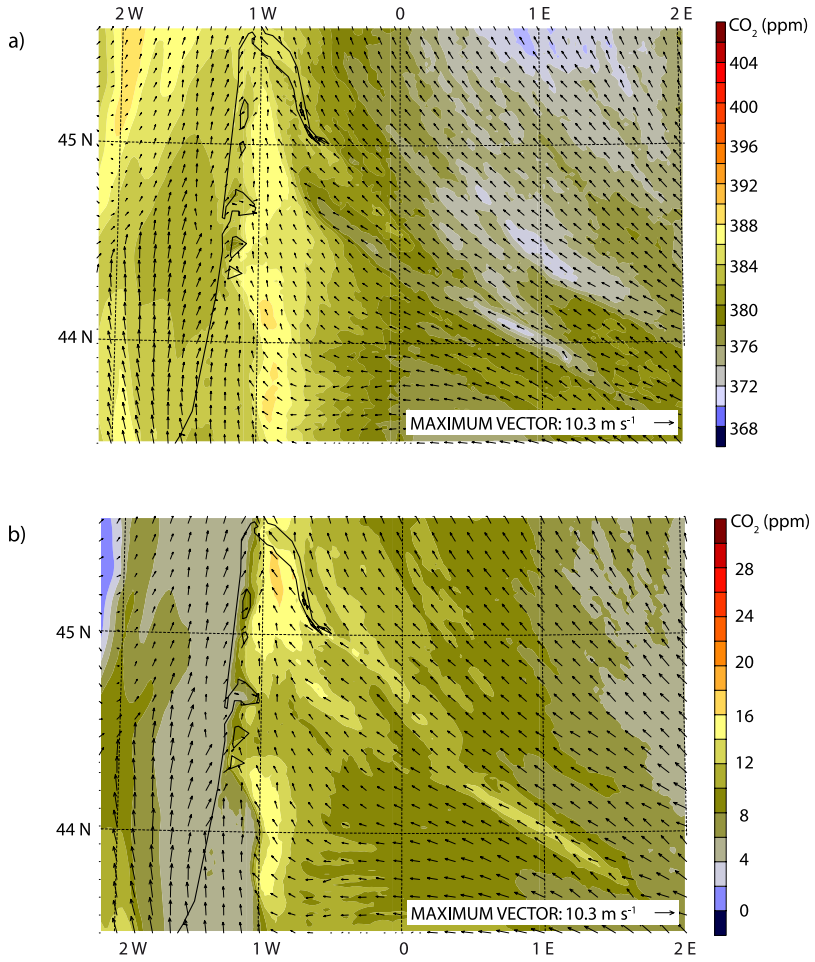

Figure 3. Near-surface (a) total and (b) respired CO_2 tracer distribution and horizontal winds over the domain at 1400 on 27 May.

outer domain in Spain (e.g., Bilbao city), from which emission plumes can be advected into the inner domain.

4.2. Case 2 (6 June 2005)

[35] During the day, high-level clouds (cirrus) arrived from the north. The wind was weak from NW at all levels (5 to 10 kt) and regular during the day. The air temperature was lower than in the 27 May case (20–25°C). The western part of the region was under the influence of a high-pressure system centered over the Atlantic Ocean.

[36] During the night, a weak land breeze transported respired CO_2 to the marine boundary layer. Weak NW winds occurred over the CERES region throughout the day, with an enhancement of the onshore winds due to a sea breeze. Similar to the previous case, anthropogenic emissions play a minor role compared to the strong fluxes from an even more active biosphere this day (cropland). There is a horizontal CO_2 gradient across the coastline, but not as far inland as in the 27 May case. Since 6 June day was cooler, respiration was weaker (see Figure 4), while photosynthesis was stronger due to phenology (mostly caused by the cropland growth, see next section), so that NEE fluxes were significantly higher than in the 27 May case. Mainly due to the lack of wind convergence (as in the 27 May case) there was not a very strong CO_2 horizontal gradient in the low atmosphere over the land.

4.3. Comparison With Observations

[37] In order to assess how realistic WRF-VPRM results are, we compared the model results with multiple observations of mixing ratios, fluxes and meteorological parameters. As we stated before, the largest source of the spatiotemporal variability in CO_2 fluxes is the biospheric flux distribution calculated by VPRM.

[38] A comparison of simulated NEE with half hourly averaged eddy covariance measurements at six different sites is shown in Figure 4 for both simulated days. For a description of these sites, see Table 2. The stations belong to different vegetation types, which generate differences in fluxes and micrometeorology. Large spatial differences in NEE are seen on 27 May for example between the nearly inactive cropland sites (LACS and MARM) and the more active cropland sites (AURA and LAMA). This difference is reproduced in VPRM only due to spatial differences in the satellite indices EVI and LSWI. Large temporal differences are also seen between the two days for the cropland sites LACS and MARM due to phenology. This shows that VPRM is able to capture the dominant patterns of spatiotemporal variability, with temporal scales ranging from

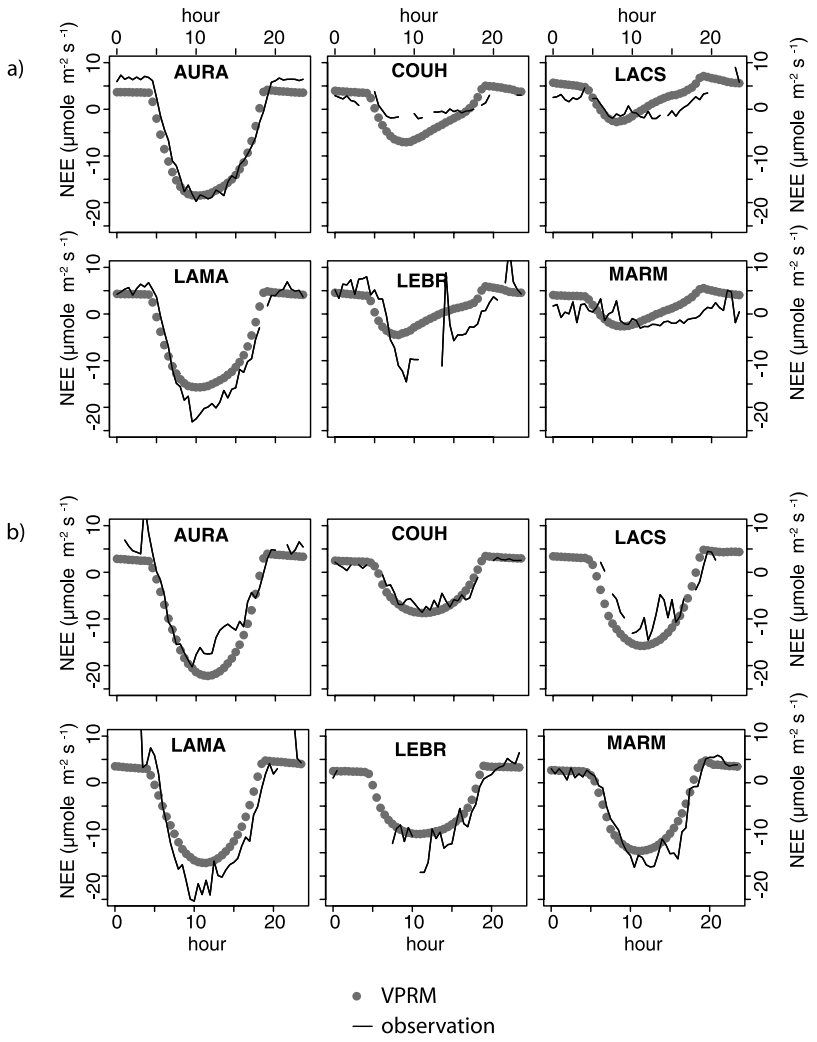

Figure 4. Comparison of VPRM NEE fluxes versus eddy-flux tower measurements for (a) 27 May and (b) 6 June.

diurnal (response to light) to seasonal (phenology), and with spatial scales starting at the size of the footprint of an eddy flux tower.

[39] The next component of the modeling system is the transport within WRF, which is intimately related to advective and mixing processes that are apparent in meteorological soundings. To validate this part of WRF, we first compare WRF results for meteorological parameters to radiosoundings. During the CERES campaign three sites, La Cape Sud, Bordeaux and Toulouse (Figure 1), were used for regular radiosoundings. Here we focus mainly on La Cape Sud, because it is at the center of the domain, located not very far from the coastline, it is equipped with surface flux measurements, and it was frequently targeted by the radiosoundings and also the aircraft for flybyes. Comparisons between WRF results and the observations at La Cape Sud are given in Figure 5 for the early morning and afternoon of 27 May (case 1) and in Figure 6 for the morning and afternoon of 6 June (case 2).

[40] The comparison of potential temperature profiles shows the ability of WRF to simulate the nocturnal stable layer as well as the afternoon convective boundary layer development reasonably well. Especially the model's deep boundary layer over the forest is confirmed by measurements (the site is in a small cropland patch, but the larger surrounding area is the Les Landes forest). The model results also show a good agreement for moisture distribution with height. The wind profile comparisons shown in Figure 5a demonstrate that the model correctly predicts the direction and magnitude of the winds in the morning. In the afternoon there is some disagreement, with WRF horizontal winds in the PBL slightly turned westward compared the

Table 2. Flux Measurement Sites[a]

Site	Label	Latitude	Longitude	Altitude, m	Land Use Type
Auradé	AURA	43°33.0′	+1°06.5′	245	rapeseed
Couhins	COUH	44°45.6′	−0°33.6′	25	vineyard
La Cape Sud	LACS	44°25′	−0°37′	70	beans
Lamasquère	LAMA	43°29.6′	+1°14.2′	180	wheat
Le Bray	LEBR	44°43′	−0°46′	60	pine forest
Marmande	MARM	44°26.9′	+0°12.6′	21	maize

[a]See http://carboregional.mediasfrance.org.

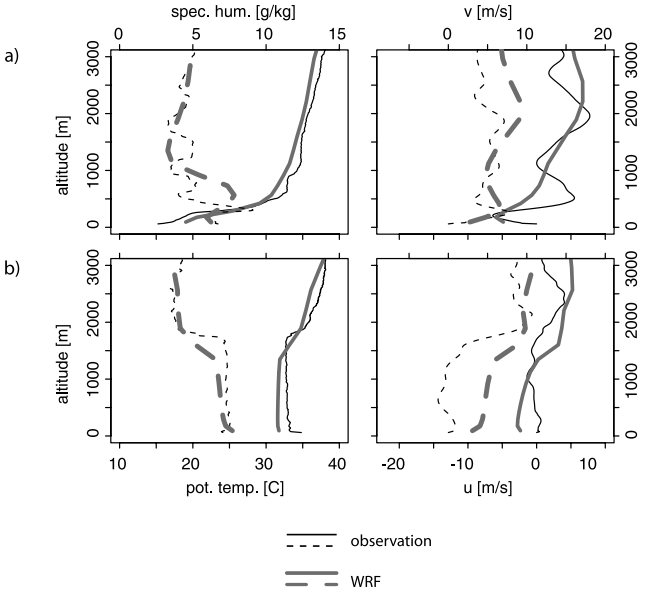

Figure 5. Comparison of WRF results with radiosonding data for 27 May at (a) 0500 and (b) 1400 at La Cape Sud.

observed ones (Figure 5b). A similar behavior was found for radiosondings at Bordeaux, which might indicate a less perfect simulation of the sea-land breeze.

[41] On 6 June we see a quite good agreement between the model and the observation for thermodynamic variables, potential temperature and specific humidity, but the model has a slight dry bias just above the PBL (Figures 6a and 6b). Also the PBL height is slightly overestimated in the evening, while during midday it is very well captured by the model. Regarding the horizontal winds, WRF shows quite reasonable results at both times. The comparison at Bordeaux and Toulouse (not shown) indicate similar performance of WRF for this day.

[42] The final step is the direct comparison of WRF simulated tracers with measurement. Undoubtedly comparisons against aircraft measurements can clarify more aspects of the regional atmospheric CO_2 distribution. During 27 May a morning flight and an afternoon flight were made to capture different stages of the convective PBL development. Here we only present results from the second flight. To facilitate interpretation of the aircraft measurements, they are presented in Figures 7 and 8 as a vertical cross-section (height versus cumulative horizontal distance), with lines indicating the aircraft path and colors indicating the mixing ratio distribution. Figure 7a shows the CO_2 measured by the MetAir's DIMO aircraft together with the WRF results. The flight was started at 1230 and lasted 4.6 hours. As can be seen from the map of the flight, the aircraft had a complex route over the Les Landes forest, cropland areas and the coastal ocean. The general strategy was to follow the air in a Lagrangian sense [*Lin et al.*, 2004] as it was advected in a northwest direction over the area. This was aided by a constant level balloon that was released at La Cape Sud when the aircraft flew by, and revisited by the aircraft later about 50 km northwest [*Dolman et al.*, 2006]. The above mentioned prominent horizontal CO_2 gradient within PBL in the west-east direction displayed in Figure 2d) was observed by the aircraft (red arrows on the Figure 7a). The model predicts the low CO_2 concentration area within PBL over the cropland region (the red part of the trajectory curve on Figure 7c). Another low concentration CO_2 area is observed and also was captured by WRF-VPRM at the end of the flight above the forest area (cumulative distance range 700–750 km). However, here the model slightly underestimates PBL height.

[43] Two sections of the flight were in the vicinity of the shoreline above the ocean (the blue curves on Figure 7c). Within 150–250 km and 600–700 km cumulative distance range the aircraft flew at few hundred meters height above the ocean. As seen from the plots WRF shows some underestimation ($\approx$3–4 ppm) of CO_2 concentration for these parts of the flight path. As above mentioned WRF simulated a flow of an air mass with low CO_2 content near the coast (Figure 3a). Since we do not have any CO_2 measurements over a large area of the ocean it is difficult to determine whether this low-concentration air mass is real, but shifted in location slightly.

[44] Figure 7b shows the same kind of comparison but for another atmospheric constituent: moisture. Over the coastline area where CO_2 profile shows disagreement, the simulated moisture exhibits a similar bias, only that it is overestimated in this case. Together with the radiosounding comparisons this suggests that the disagreement for CO_2 concentration over the coastal area is mainly a transport problem rather than inaccurate estimation of CO_2 fluxes. Potential temperature (not shown) indicated good agreement between WRF and the aircraft data for this flight. For the shorter morning flight over the land (not shown), WRF captured both meteorological and CO_2 distributions rather well.

[45] Figure 8 presents the model and the aircraft CO_2 "cross-section" plots for 6 June. The flight started at around 0900, and lasted for 4 hours. Also this flight was executed

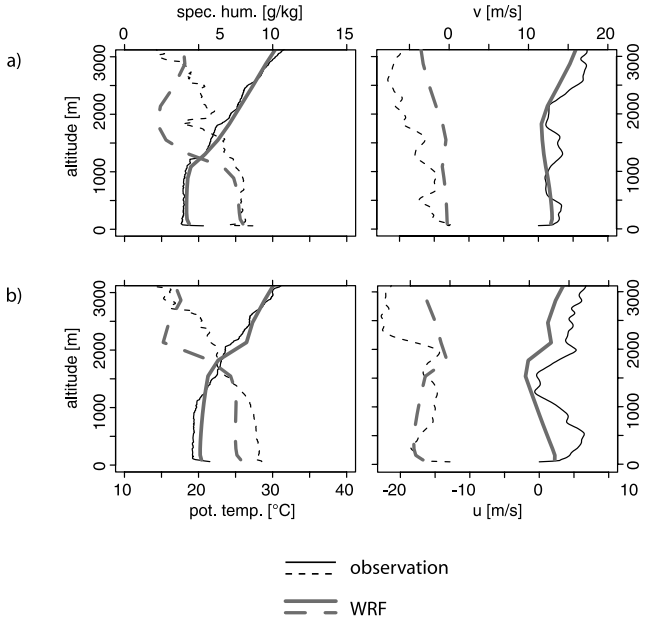

Figure 6. Similar to Figure 5, but for the 6 June case at (a) 1100 and (b) 1700.

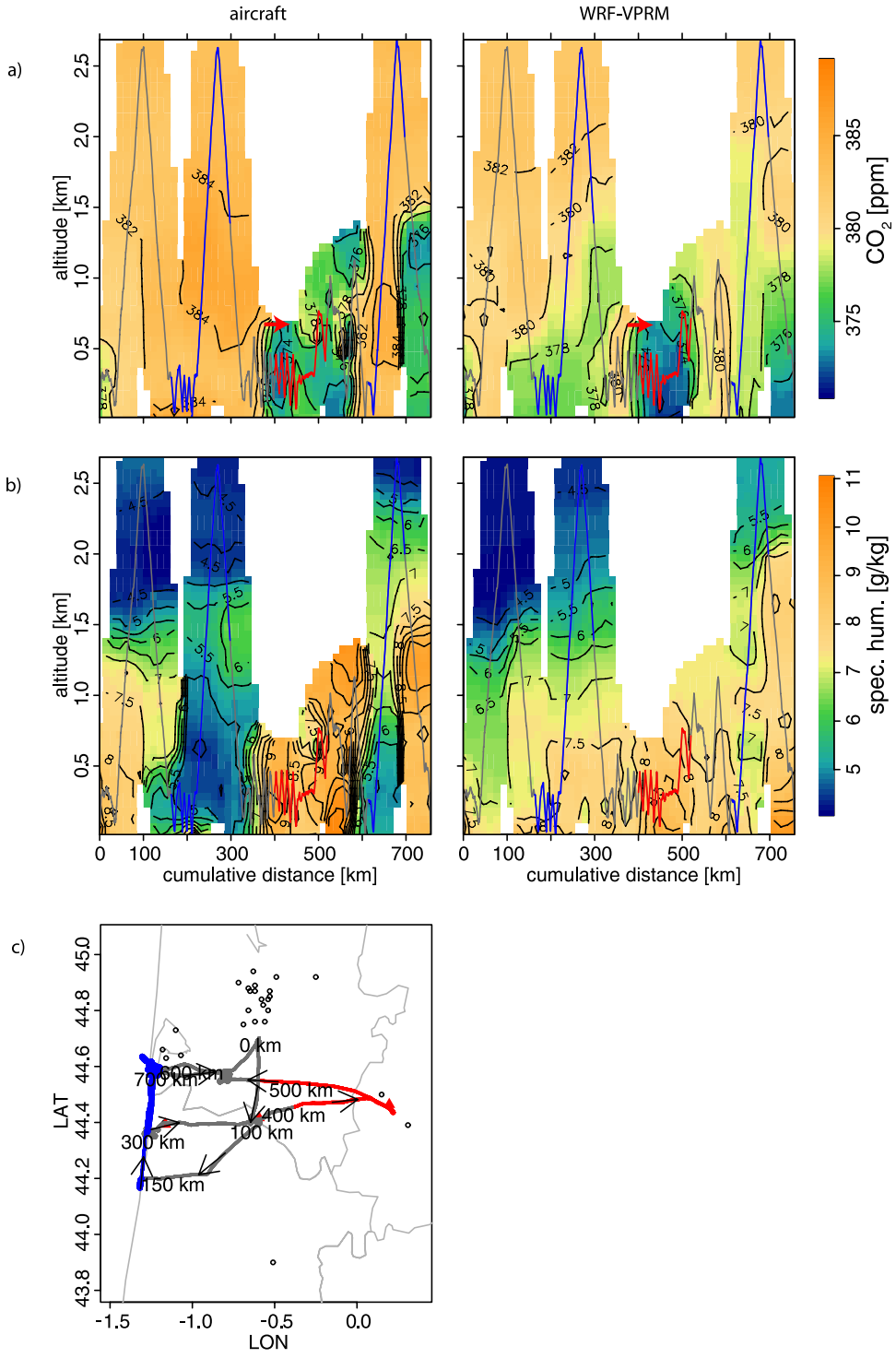

Figure 7. Comparison of (a) CO_2 and (b) moisture profiles between the aircraft measured and predicted by WRF-VPRM for 27 May. (c) Horizontal trajectory of the aircraft flight. The different colors on the vertical (sawtooth like) and horizontal aircraft trajectory curves show different parts of the flight. Contours and colors indicate tracer mixing ratio as interpolated from the measurements using the squared inverse of the distance as weighting (aspect ratio vertical/horizontal is 1/200).

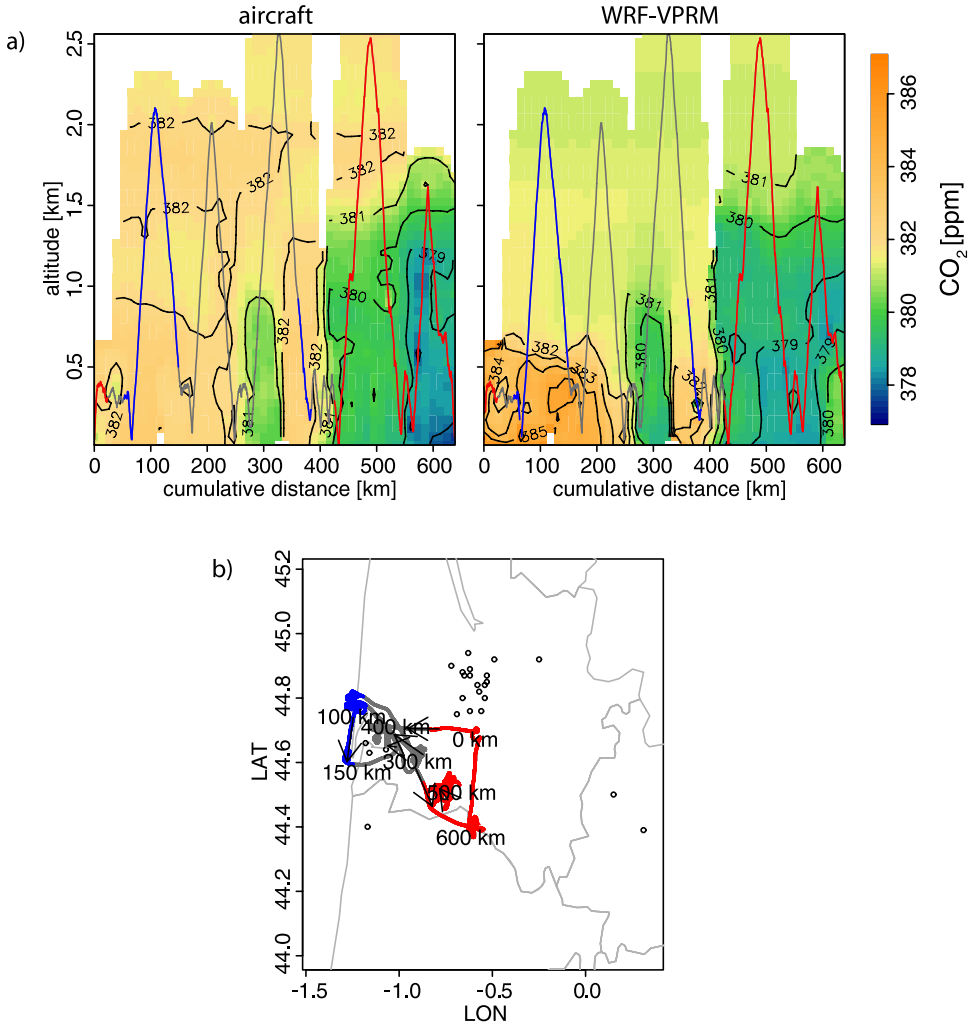

Figure 8. Similar to Figure 7, but for 6 June showing (a) the comparison of CO_2 profiles between the aircraft measurements and WRF-VPRM results and (b) the horizontal trajectory of the aircraft flight.

as a Lagrangian, following an air mass from north of Arcachon to La Cape Sud (cumulative distance range 100–600 km on the aircraft trajectory graph in Figure 8b). As the air is transported farther inland, and as time progresses from morning to noon, observation and model both show a pronounced change in the mixed layer CO_2 concentration as well as a deepening mixed layer. Two profiles with boundary layer depletion in CO_2 were measured by the aircraft (Figure 8a). The one at km 300 with ~1 km high PBL is very well simulated by the model. The profile near the end of the flight was captured by the model, however both PBL height and CO_2 concentration show a slight bias. The comparison for meteorological variables such as potential temperature and moisture shows a good performance of the model, apart from the drier layer in WRF also mentioned above in context of the radiosonde comparison.

[46] In general during this day the model exhibits slightly more variability than the measurements, with an enhancement of CO_2 over and near the ocean (70–170 km cumulative distance) that was not as pronounced in the measurements. The bias near the shoreline between the model and the observation is not as high as in 27 May, probably because the measurements were made around 1000, so the sea breeze was not fully developed.

[47] Since CO_2 measurements over the coastal regions are very crucial as representative sites of a global monitoring network, there is no doubt that mesoscale model performance in such areas must be investigated further. A detailed and comprehensive assessment of the model performance is beyond the scope of this paper, but we nevertheless want to give some ideas of potential reasons for this problem. The inappropriate representation of the coastal shape due to a finite resolution results in inaccurate simulation of sea-land breeze direction and presence of low-level convergence or divergence areas [*Pielke*, 2002]. Another problem is that a numerical model's resolution for atmospheric fields is about $4\Delta x$ which is 8 km in our case, which smoothes out the sharp temperature gradients associated with the coastline. The airborne measurements over the ocean where made however in close proximity of the coast (about 100 m) due to safety reasons, so it matters where coastline is and the gradients are simulated in the model. Further, the ECMWF sea surface temperature might not be representative on the scales relevant for our simulation. A future option would be to use higher resolution SST data from satellites.

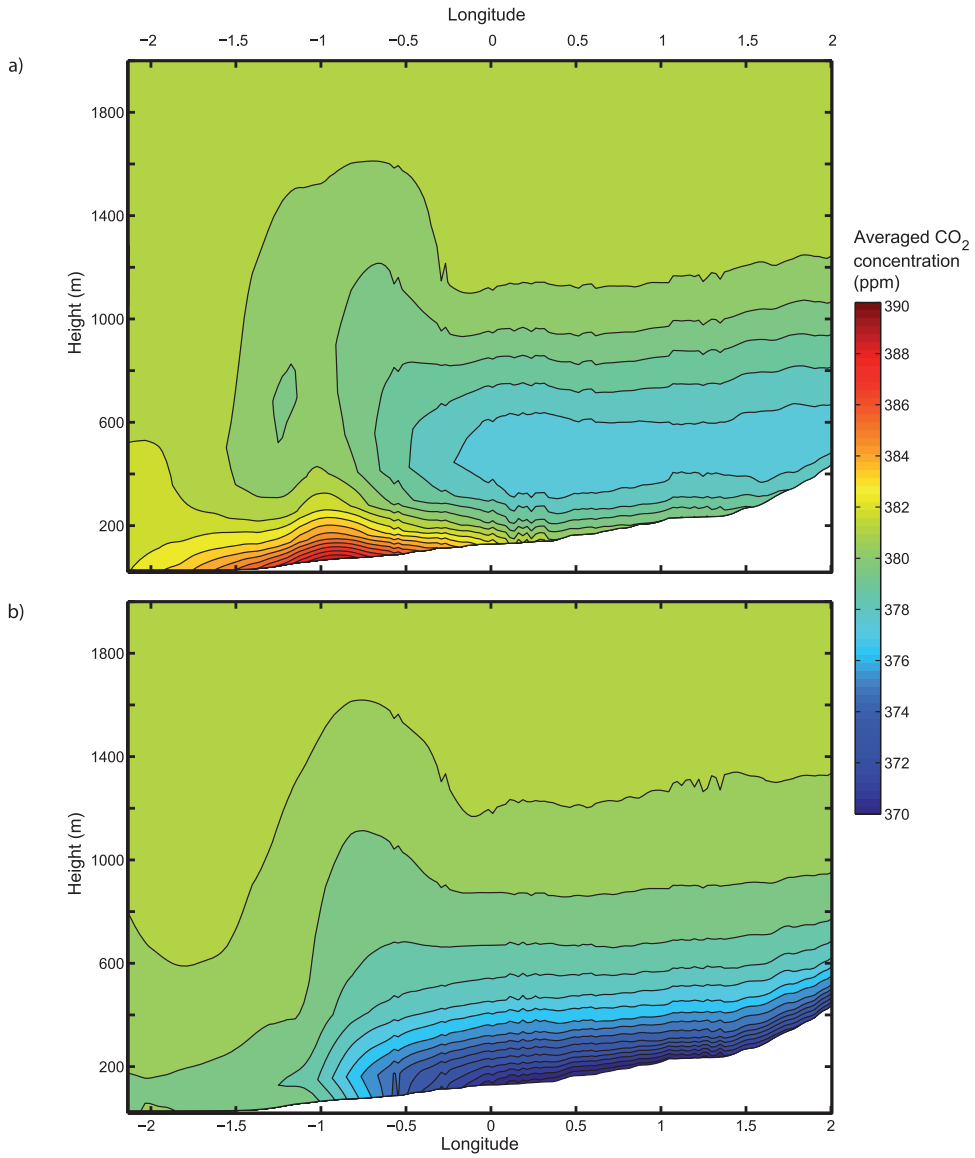

Figure 9. The 24-hour- and latitudinally averaged CO_2 concentration distribution for the 27 May case, WRF-VPRM run with (a) diurnal CO_2 fluxes and (b) hourly averaged constant CO_2 fluxes. Height is shown as above mean sea level.

[48] As presented above for the given region and the discussed days, the regional patterns of biospheric fluxes together with mesoscale transport processes play a dominant role in modifying the atmospheric CO_2 distribution. However, there is some variability, especially above PBL, also caused by spatial gradients in the lateral and initial boundary fields that are associated with synoptic scale differences. To assess the impact of this, we also did test runs where CO_2 was initialized with a horizontally homogenous profile based on aircraft observations from the previous day. The results showed a slight degradation, indicating that it is better to use initial and lateral boundary conditions that resolve synoptic scale CO_2 disturbances. In general such disturbances are important for some cases and areas [*Chevillard et al.*, 2002]. For longer-term simulations of course there is a practical advantage in using global model boundary fields, since usually there is no regular measuring CO_2 profiles in the previous day or upstream of the domain.

5. Discussions and Conclusions

[49] We introduced WRF-VPRM as a new modeling system that couples a diagnostic biosphere model, a high-resolution emission inventory, and realistic boundary conditions from a global CO_2 transport model with a weather forecasting model in order to simulate fluxes and concentrations of CO_2 at high spatial and temporal resolution. We applied the modeling tool for two different days of the CERES regional experiment, with different conditions in both meteorology and biospheric activity. Setting up WRF-VPRM initially for the CERES experiment is targeted at testing the modeling system, since the large amount of

experimental data allowed an extensive validation. The comparison with measurements of different meteorological parameters and tracers, including CO_2 mixing ratios measured by aircraft, demonstrate that WRF-VPRM is capable to simulate their spatial and temporal distribution with reasonable skill. Although VPRM is a relatively simple biospheric model, it properly captures the relevant scales of variability, certainly for regional applications. The fact that VPRM performs so well is also partly due to the fact that clear sky conditions were chosen. As mentioned above, under conditions with cumulus cloud development inaccuracies might be expected due to biased radiation fields, since cumulus clouds might not be always properly resolved within WRF. The development of the PBL with its impact on the distribution of CO_2 through vertical mixing is well represented. Most importantly, due to its high spatial resolution the model captures mesoscale transport processes such as the sea-land breeze circulation. Although the exact magnitude and direction of the sea breeze circulation is not always simulated perfectly, the main flow patterns are reasonably resolved.

[50] An important conclusion of this analysis however is that measurements made at coastal stations do not always see large-scale representative CO_2 signals in onshore air flows, but that in cases of a sea breeze circulation the spatiotemporal patterns show a strong mesoscale character. The tagged tracers used within WRF-VPRM for different sources or sinks of CO_2 such as respiration and photosynthesis demonstrated for the case of 27 May that CO_2 respired over the land biosphere and then transported to the ocean during the night is partially recirculated during daytime in onshore winds, a process that is strongly amplified with the sea breeze. Changes of wind direction that are associated with synoptic events are usually uncorrelated with biospheric activity. However, in case of sea-land breeze circulations, they are strongly correlated, with flux from the biosphere to the atmosphere during night coinciding with land breeze, and biospheric uptake during day time coinciding with sea breeze.

[51] This temporal covariance between transport and flux during the growing season is likely to cause large errors in simulations in which these processes are not properly represented, very similar to the diurnal rectifier effect [*Denning et al.*, 1996]. Even if a sea breeze is not fully developed, there is still a significant mesoscale modification of the large scale flow that covaries with the temporal pattern of biospheric exchange. A similar phenomenon is likely to occur due to mountain-valley circulations, where the diurnal change in winds is covarying with photosynthesis of the vegetation. Such covariances, for which the term "3-D rectifier effect" has been suggested for the Western Mediterranean Basin [*Perez-Landa et al.*, 2006], are principal in nature, since they relate to the biosphere and the transport being driven by the same process, solar radiation. When interpreting data from sites influenced by such mesoscale rectification phenomena in coarse modeling frameworks as it is done for example in inversions [*Kaminski et al.*, 1999; *Gurney et al.*, 2002], such cases have to be removed from the analysis, or an additional uncertainty has to be assigned to account for the inappropriate representation in the model.

[52] In order to estimate the magnitude of the effect we have run WRF-VPRM with the same setup, but with temporally averaged CO_2 fluxes (24 hour averages). The results from the runs with diurnal and with constant fluxes are given in Figures 9a and 9b. Figure 9a clearly shows the two kinds of rectification processes: the diurnal (vertical) rectifier, resulting in a difference in the vertical gradients in the boundary layer over land, and the 3-D rectifier as discussed here related to mesoscale circulation in the coastal area, resulting in a strong horizontal gradient near the coast of about 10 ppm over a distance of 50–100 km. The strong buildup of CO_2 near longitude $-1°$E is seen in Figure 3b as well, which confirms that it is the 3-D rectifier effect caused by the respired CO_2 being recirculated. The distribution using time averaged fluxes (Figure 9b) in contrast does not contain any similar vertical or horizontal gradient in the vicinity of the coast due to the lack of covariance between CO_2 fluxes and the meteorology. Within the 2007 CERES extensive operational period, there are two towers operational for continuous CO_2 measurements in this domain: one near Biscarosse in the close vicinity of the coastline and a second one near Bellegarde, about 200 km farther inland, northwest of Toulouse. This will provide an opportunity for examination of this effect over a yearlong time period.

[53] It is obvious that the WRF-VPRM modeling system needs further validation, including simulations over longer time periods in order to better understand all its strengths and weaknesses. As shown, the main reason for discrepancies between CO_2 observations and model results is not the VPRM performance, but is related to remaining inaccuracies of transport within WRF. In this context, aircraft measurements of CO_2 and other variables, especially when done with multiple profiles characterizing the distributions at mesoscales, seem very promising for future research campaigns in order to understand regional carbon budget and also validate high-resolution transport models.

[54] Future applications of WRF-VPRM will focus on the near field of measurement data continuously obtained in different regions and seasons at such sites as tall towers. Investigating mesoscale transport at continental measurement stations, which are increasing in numbers within the global CO_2 monitoring network, is essential for the interpretation of the data. There is no way around closing the existing gap between the local measurements and the global modeling tools. Mesoscale models are an essential tool for quantifying the representation error of the coarse models. Further, in addition to a diagnostic role, the combination of WRF-VPRM and STILT will be used in the near future as an inverse modeling system to retrieve regional scale estimates of surface fluxes from long-term observations of CO_2.

[55] **Acknowledgments.** The authors would like to thank W. C. Skamarock from NCAR for providing us with modified WRF code with tracer transport implementation and also the WRF developers for the user support. We are grateful to all the CERES community for providing measurement results and global CO_2 model data, A. Jordan and M. Rothe from the GasLab at MPI BGC for trace gas analysis of flask samples, E. Ceschia from CESBIO for flux data, S. Reis from IER for the CO_2 emission inventory, and also the CNRM 4M team for radiosoundings at La Cape Sud. The CERES campaign was supported by the Sixth Framework Programme of the European Commission (Directorate-General Research) through CarboEurope-IP, contract GOCE-CT-2003-505572.

References

Bakwin, P. S., C. Zhao, W. Ussler III, P. P. Tans, and E. Quesnell (1995), Measurements of carbon dioxide on a very tall tower, *Tellus, Ser. B*, *47*, 535–549.

Chevillard, A., U. Karstens, P. Ciais, S. Lafont, and M. Heimann (2002), Simulation of atmospheric CO_2 transport in Europe and Siberia using the regional scale model REMO, *Tellus, Ser. B*, *54*, 872–894.

Denning, S. A., D. A. Randall, G. J. Collatz, and P. J. Sellers (1996), Simulations of terrestrial carbon metabolism and atmospheric CO_2 in a general circulation model. 2. Simulated CO_2 concentrations, *Tellus, Ser. B*, *48*(4), 543–567.

Denning, S. A., M. Nicholls, L. Prihodko, I. Baker, P. L. Vidale, K. Davis, and P. Bakwin (2003), Simulated variations in atmospheric CO_2 over a Wisconsin forest using a coupled ecosystem-atmosphere model, *Global Change Biol.*, *9*, 1241–1250.

Dolman, A. J., et al. (2006), CERES, the CarboEurope Regional Experiment Strategy in Les Landes, south west France, May–June 2005, *Bull. Am. Meteorol. Soc.*, *87*(10), 1367–1379.

Gangoiti, G., M. M. Millan, R. Salvador, and E. Mantilla (2001), Long-range transport and re-circulation of pollutants in the western Mediterranean during the project Regional Cycles of Air Pollution in the west-central Mediterranean area, *Atmos. Environ.*, *35*(36), 6267–6276.

Gerbig, C., J. C. Lin, S. C. Wofsy, B. C. Daube, A. E. Andrews, B. B. Stephens, P. S. Bakwin, and C. A. Grainger (2003), Toward constraining regional-scale fluxes of CO_2 with atmospheric observations over a continent: 2. Analysis of COBRA data using a receptor-oriented framework, *J. Geophys. Res.*, *108*(D24), 4757, doi:10.1029/2003JD003770.

Gerbig, C., J. C. Lin, J. W. Munger, and S. C. Wofsy (2006), What can tracer observations in the continental boundary layer tell us about surface-atmosphere fluxes?, *Atmos. Chem. Phys.*, *6*, 539–554.

Gurney, K., et al. (2002), Towards robust regional estimates of CO_2 sources and sinks using atmospheric transport models, *Nature*, *415*, 626–630.

Jung, M., K. Henkel, M. Herold, and G. Churkina (2006), Exploiting synergies of global land cover products for carbon cycle modeling, *Remote Sens. Environ.*, *101*(4), 534–553, doi:10.1016/j.rse.2006.01.020.

Kaminski, T., M. Heimann, and R. Giering (1999), A coarse grid three-dimensional global inverse model of the atmospheric transport: 2. Inversion of the transport of CO_2 in the 1980s, *J. Geophys. Res.*, *104*, 18,555–18,581.

Lin, J. C., C. Gerbig, S. C. Wofsy, A. E. Andrews, B. C. Daube, C. A. Grainger, B. B. Stephens, P. S. Bakwin, and D. Y. Hollinger (2004), Measuring fluxes of trace gases at regional scales by Lagrangian observations: Application to the CO_2 Budget and Rectification Airborne (COBRA) study, *J. Geophys. Res.*, *109*, D15304, doi:10.1029/2004JD004754.

Lu, L., A. S. Denning, M. A. da Silva-Dias, P. da Silva-Dias, M. Longo, S. R. Freitas, and S. Saatchi (2005), Mesoscale circulations and atmospheric CO_2 variations in the Tapajós Region, Pará, Brazil, *J. Geophys. Res.*, *110*, D21102, doi:10.1029/2004JD005757.

Mahadevan, P., S. C. Wofsy, D. M. Matross, X. Xiao, A. L. Dunn, J. C. Lin, C. Gerbig, J. W. Munger, V. Y. Chow, and E. W. Gottlieb (2007), A satellite-based biosphere parameterization for net ecosystem CO_2 exchange: Vegetation Photosynthesis and Respiration Model (VPRM), *Global Biogeochem. Cycles*, doi:10.1029/2006GB002735, in press.

Matross, D., et al. (2006), Etimating regional carbon exchange in New England and Quebec by combining atmospheric, ground-based, and satellite data, *Tellus, Ser. B*, *58*, 344–358.

Perez-Landa, G., P. Ciais, G. Gangoiti, J. L. Palau, A. Carrara, B. Gioli, F. Miglietta, M. Schumacher, M. M. Millan, and M. J. Sanz (2006), Mesoscale circulations over complex terrain in the Valencia coastal region, Spain, part 2: Linking CO_2 surface fluxes with observed concentrations, *Atmos. Chem. Phys. Discuss.*, *6*, 2853–2895. (Available at http://www.atmos-chem-phys-discuss.net/6/2853/2006/)

Peylin, P., P. J. Rayner, P. Bousquet, C. Carouge, F. Hourdin, P. Heinrich, P. Ciais, and AEROCARB Contributors (2005), Daily CO_2 flux estimates over Europe from continuous atmospheric measurements: 1, Inverse methodology, *Atmos. Chem. Phys. Discuss.*, *5*, 1647–1678.

Pielke, R. (2002), *Mesoscale Meteorological Modeling*, 2nd ed., 676 pp, Academic, San Diego, Calif.

Rayner, P. J., M. Scholze, W. Knorr, T. Kaminski, R. Giering, and H. Widmann (2005), Two decades of terrestrial carbon fluxes from a carbon cycle data assimilation system (CCDAS), *Global Biogeochem. Cycles*, *19*, GB2026, doi:10.1029/2004GB002254.

Rödenbeck, C., S. Houweling, M. Gloor, and M. Heimann (2003), CO_2 flux history 1982–2001 inferred from atmospheric data using a global inversion of atmospheric transport, *Atmos. Chem. Phys.*, *3*, 1919–1964.

Sarrat, C., et al. (2007a), Atmospheric CO_2 modeling at the regional scale: Application to the CarboEurope Regional Experiment, *J. Geophys. Res.*, *112*, D12105, doi:10.1029/2006JD008107.

Sarrat, C., et al. (2007b), Atmospheric CO_2 modeling at the regional scale: An intercomparison of 5 meso-scale atmospheric models, *Biogeosci. Discuss.*, *4*, 1923–1952.

Schmitgen, S., H. Geiß, P. Ciais, B. Neininger, Y. Brunet, M. Reichstein, D. Kley, and A. Volz-Thomas (2004), Carbon dioxide uptake of a forested region in southwest France derived from airborne CO_2 and CO measurements in a quasi-Lagrangian experiment, *J. Geophys. Res.*, *109*, D14302, doi:10.1029/2003JD004335.

Skamarock, W. C., J. B. Klemp, J. Dudhia, D. O. Gill, D. M. Barker, W. Wang, and J. G. Powers (2005), A description of the Advanced Research WRF Version 2, Tech. Note NCAR/TN-468_STR, Natl. Cent. for Atmos. Res., Boulder, Colo.

Tans, P., I. Fung, and T. Takahashi (1990), Observational constraints on the global atmospheric CO_2 budget, *Science*, *247*, 1431–1438.

van der Molen, M. K., and A. J. Dolman (2007), Regional carbon fluxes and the effect of topography on the variability of atmospheric CO_2, *J. Geophys. Res.*, *112*, D01104, doi:10.1029/2006JD007649.

Xiao, X., D. Hollinger, J. Aber, M. Goltz, E. A. Davidson, Q. Zhang, and B. Moore III (2004), Satellite-based modeling of gross primary production in an evergreen needleleaf forest, *Remote Sens. Environ.*, *89*(4), 519–534.

R. Ahmadov, C. Gerbig, S. Koerner, and R. Kretschmer, Max Planck Institute for Biogeochemistry, Hans-Knoll Str. 10, Jena, D-07745, Germany. (rahmadov@bgc-jena.mpg.de)

A. J. Dolman, Department of Hydrology and Geo-environmental Sciences, Vrije Universiteit Amsterdam, De Boelelaan 1105, 1081 HV Amsterdam, Netherlands.

B. Neininger, MetAir, Sonnenberg 27, CH-6313 Menzingen, Switzerland.

C. Sarrat, CNRM Meteo France, 42 Avenue Gaspard Coriolis, F-31057 Toulouse, France.